Automated Assessment of Loss of Consciousness Using Whisker And Paw Movements During Anesthetic Dosing in Head-Fixed Rodents

Jingzhi An*, Francisco J. Flores*, Suhasa B. Kodandaramaiah, Isabella Dalla Betta, Ksenia Nikolaeva, Edward S. Boyden, Craig R. Forest and Emery N. Brown.

***Abstract*—The precise identification of loss of consciousness (LOC) is key to studying the effects of anesthetic drugs in neural systems. The standard behavioral assay for identifying LOC in rodents is the Loss of Righting Reflex (LORR), assessed by placing the animal in the supine position every minute until it fails to right itself. However, this assay cannot be used when the rodents are head-fixed, which limits the use of powerful techniques such as multi-electrode recordings, *in-vivo* patch clamp, and neuronal imaging. In these situations, an alternative way to assess LOC is needed. We propose that loss of movement (LOM) in whiskers and paws of head-fixed animals can be used as an alternative behavioral assay in head-fixed animals. Unlike LORR, LOM in whiskers and paws is much harder to detect by visual inspection. Therefore, we developed a method to automatically assess for LOM of whiskers and paws in head fixed rodents during *in vivo* patch clamp recordings. Our method uses an algorithm based on optical flow and point-process filtering which can be run on images acquired on regular cameras at low frame-rates. We show that the algorithm can achieve at least comparable accuracy in detecting LOC when compared with consensus among human observers, as well as improved precision when compared with individual observers. In the future, we aim to to expand the method to detect more behavioral end-points during anesthesia such as paradoxical excitation. Eventually, we hope to enable multi-modal anesthesia studies, which incorporates behavioral and neurophysiological data.**

***Index Terms*—anesthesia, optical flow, point-process, motion detection, image feature extraction.**

I. Introduction

Precisely identifying loss of consciousness (LOC) is key to studying its neural correlates. In clinical practice, simple tests such as responsiveness to verbal commands are often used. In research settings, more complex tasks such as response to combinations of auditory stimuli can be used to define LOC [1]. These behavioral assays are used in multi-modal anesthesia studies in combination with with EEG, fMRI, and other physiological recordings [2] to examine mechanisms by which anesthetic drugs produce LOC.

In contrast to humans, the repertoire of behavioral assays for LOC in rodents is much more limited. The standard measure is the Loss of Righting Reflex (LORR), which is assessed by quickly placing the animal in the supine position every minute until it fails to right itself [3]. While LORR is a reliant measure, it is incompatible with techniques with high temporal and spatial resolutions that can be used in rodents to obtain even more insights about anesthetic actions and LOC. For example, targeted multisite recordings can be used to assess the temporal dynamics of large cortical and subcortical networks during LOC [4]; *in vivo* patch clamp recordings [5] can be used to study the effects of anesthetics on membrane potential, and invasive neuronal imaging techniques such as calcium imaging [6] can be used to produce highly detailed observations of neurophysiological dynamics during anesthesia. These methods all require that the animal be head-fixed, which precludes the possibility of performing the LORR assessment.

We propose a new behavioral assay to assess LOC in head-fixed rodents using the loss of movement (LOM) in whiskers and paws. This proposal is inspired by previous work in which we established a strong correlation between LORR and LOM [4]. We demonstrate a proof-of-concept of this new assay in head-fixed rodents undergoing *in vivo* whole-cell current clamp recordings. Because LOM in whiskers and paws is challenging to detect by visual inspection, we developed an algorithm based on optical flow and point-process filtering to perform this task automatically.

II. Methods.

A. Animal preparation and video acquisition

All procedures were performed in agreement with federal, state, and local regulations. The protocol #0113-008-16 was approved by the Committee on Animal Care at the Massachusetts Institute of Technology. The methods have been published in detail in Kodandaramaiah et al. [5]. In short, adult male C57BL/6 mice, 8 weeks old, were implanted with metallic head plates under anesthesia and sterile conditions. After a week of post-surgical recovery, where analgesics were administered, the mice were behaviorally acclimated to the head-fixed set-up in sessions of increasing duration from 10 minutes to 30 minutes over a period of 7 days. Mice were given diluted condensed milk during the acclimation sessions

*These authors contributed equally to this work.

JA and ENB are with the Harvard-MIT Division of Health Science and Technology; KN and ENB are with Institute for Medical Engineering; ESB is with Media Lab, McGovern Institute for Brain Research, and Department of Biological Engineering; FJF and ENB are with Picower Institute for Learning and Memory; all at Massachusetts Institute of Technology, Cambridge, MA, USA. FJF and ENB are with the Department of Anesthesia, Critical Care, and Pain Medicine, Massachusets General Hospital and Harvard Medical School, Boston, MA, USA. SBK and CRF are with the Department of Mechanical Engineering, University of Minnesota-Twin Cities, Minneapolis, MN, USA. IDB is with Wellesley College, Wellesley, NA, USA. CRF is with G. W. Woodruff School of Engineering, Atlanta, GA, USA.

Funding: A*STAR National Science Scholarship (MD-PhD) to JA. New York Stem Cell Foundation and National Science Foundation to ESB. National Institutes of Health to ENB, CRF and SBK. MGH and Picower Institute to ENB. McGovern Institute Neurotechnology Fund to SBK.

978-1-5386-3646-6/18/$31.00 ©2018 IEEE

to minimize stress and provide positive reinforcement. On the day of the experiment, an indwelling cannula was placed in the peritoneal cavity, and the mice were placed in the head-fixed recording set-up for *in vivo* whole-cell current clamp [5].

A scientific grade camera (Firefly MV 0.3 MP Mono FireWire 1394a, Flir Machine Vision) was installed in front of the mice, together with an off-the-shelf infrared illumination source. The camera's shutter was triggered at 20 frames per second using a computer interface board (NIDAQ NI-USB 6259, National Instruments) controlled via custom-written LabView Software (National Instruments). Frames were acquired at a resolution of 800×600 pixels. A copy of the trigger signal was send to the patch amplifiers for synchronization with the neurophysiological recordings. The full set-up for the experiment and video acquisition is shown in Fig. 1.

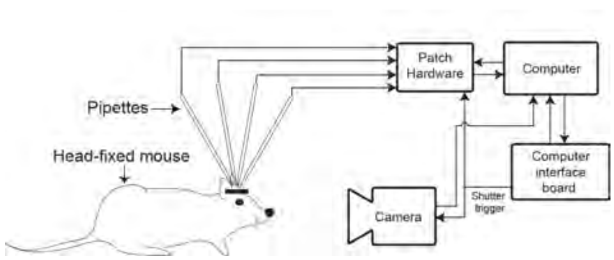

Fig. 1. Schematics of experimental setup.

The video acquisition was started simultaneously with the cellular recordings. Four minutes of baseline data were acquired before the mice were dosed with either dexmedetomidine (200 mcg/kg) or ketamine (150 mg/kg). The recordings continued for a variable period until the whole-cell state was lost.

B. Movement detection using optical flow analysis

We used optical flow to extract movement of whiskers and paws from the videos acquired. To do so, we first manually marked the regions of interest (ROIs) in the videos to include either the right paw or the right whiskers. The head-fixed set-up constrained the ROIs to a fixed area while allowing full range of movement for the whiskers and front paws. Next, we sub-sampled the ROI by a factor of two, and computed the optical flow using the Lucas-Kanade Difference-of-Gaussian algorithm as implemented in MATLAB [7], [8]. We set the number of frames for temporal smoothing to the minimum value of 3 because the original video was acquired at a low frame rate. The rest of the parameters were left at their default values (image smoothing $\sigma = 1.5$ pixels; temporal smoothing $\sigma = 1$ pixel-frame; noise threshold $= 0.0039$ arbitrary luminance units). We chose the Lucas-Kanade derivative of Gaussian algorithm because by visual inspection it produced a sparse optical flow field that was relatively unaffected by respiration-induced motions in comparison to other commonly used optical flow algorithms, such as the Horn-Schunk algorithm, or the standard Lucas-Kanade algorithm (see Fig. 2). Finally, we computed the median

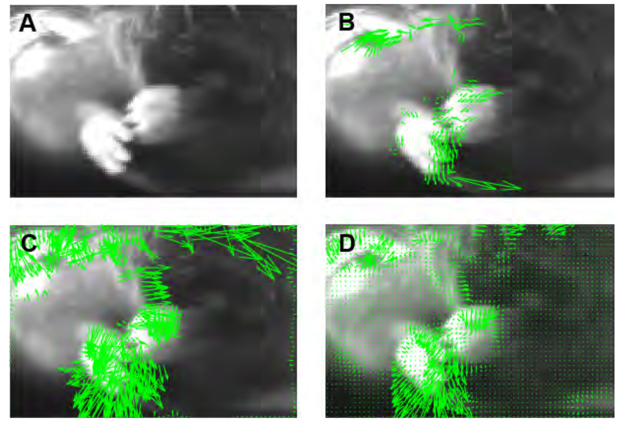

Fig. 2. Typical examples of optical flow vectors (green arrows) computed applying three different algorithms. A) ROI corresponding to the front paws. B) Lucas-Kanade Difference-of-Gaussian algorithm. C) Conventional Lucas-Kanade algorithm. D) Horn-Schunk algorithm. The scaling factor for the vectors produced by the conventional Lucas-Kanade algorithm is a fourth of the scaling factor applied to the vectors produced by the other two algorithms.

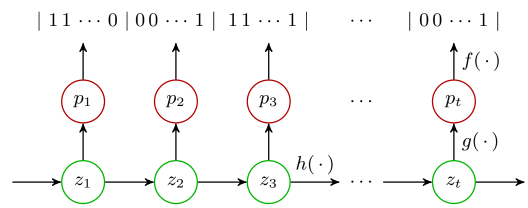

Fig. 3. State-space model for estimating the movement probabilities given median optical flow data.

magnitude of the optical flow vectors within each ROI, $y_{i,\tau}$ (where $i = w$ for whiskers and $i = p$ for paws), to summarize the optical flow measurements.

Next, we adapted a previously validated recursive variance algorithm (RVS) to convert $y_{i,\tau}$ into binary signals where zeros represent non-movement and ones represent movement [9]. This algorithm computes a recursive estimate of the local signal variance and threshold the estimate as follows:

$$\mu_{i,\tau} = \beta\mu_{i,\tau-1} + (1-\beta)y_{i,\tau} \tag{1a}$$

$$\upsilon^2_{i,\tau} = \beta\upsilon^2_{i,\tau-1} + (1-\beta)(y_{i,\tau} - \mu_{i,\tau})^2 \tag{1b}$$

$$b_{i,\tau} = \delta[\upsilon^2_{i,\tau} < \theta] \tag{1c}$$

here $y_{i,\tau}$ is the median magnitude of the optical flow vectors, $\mu_{i,\tau}$ is its local mean, $\upsilon^2_{i,\tau}$ is its local variance, and $b_{i,\tau}$ is the binary signal for whiskers ($i = w$) or paws($i = p$) at time τ. The algorithm has two parameters: the "forgetting factor" β which determines the relative influence of current data and past estimate on the current estimates; and the classification threshold θ which determines the outcome of the indicator function $\delta[\,\cdot\,]$ (which is 1 if the inequality is satisfied and 0 otherwise). We set the value of β to the globally-optimal value reported in [9] and customized the value of θ for each data set. Specifically, we applied a bisectional search algorithm to find the threshold θ such that at baseline the total duration of movement detected was between 25 – 75%.

C. Computing the movement probability (MVP)

We introduce the concept of movement probability (MVP) of the whiskers and paws which describes the instantaneous probability for movement. This is a statistically rigorous way to generate a denoised and scale-free measure from binary data [10] and can be used to classify the behavior states into LOC or non-LOC. MVP is derived based on a state-space model as shown in Fig 3. Let Δ_p be the sampling period of MVPs and Δ_b be the sampling period of the binary observations. In our model, the MVP (denoted as p_t) drives the generation of the binary observations through a binomial probability model:

$$f(p_t) = \binom{N}{k_t} p_t^{k_t}(1-p_t)^{N-k_t},$$

where $N = \Delta_p/\Delta_b$ and $k_t = \sum_{j=(t-1)N}^{tN} b_j$. p_t also relates to an underlying state z_t through a sigmoid function

$$g(z_t) = p_t = \frac{1-\exp(-z_t)}{1+\exp(-z_t)}.$$

We model the dynamics of the states as a random walk process:

$$h(z_{t-1}) = z_t = z_{t-1} + \epsilon_t$$

where ϵ_t are independent Gaussian random variables with mean 0 and variance σ_ϵ^2. This definition of the state transition provides a stochastic continuity constraint to ensure that the states (and hence the MVPs) that are close in time are close in value. We adapted the algorithm for estimating the MVPs from our previous work on point-process filters [11]. The key steps of the filtering algorithm are shown below:

$$\begin{aligned}
\text{Prediction:}\quad & z_{t|t-1} = z_{t-1|t-1}\\
& \sigma^2_{t|t-1} = \sigma^2_{t-1|t-1} + \sigma^2_\epsilon\\
\text{Update:}\quad & z_{t|t} = z_{t|t-1} + \sigma^2_{t|t}\ell_t \left.\frac{\mathrm{d}p_t}{\mathrm{d}z_t}\right|_{z_{t|t-1}}\\
& \sigma^{-2}_{t|t} = \sigma^{-2}_{t|t-1} + g_t^2[p_{t|t-1}(1-p_{t|t-1})]^{-1}
\end{aligned}$$

where

$$\begin{aligned}
z_{t|t-1} &= \mathbb{E}[z_t|k_1^{t-1}, \sigma^2_\epsilon, z_0]\\
\sigma^2_{t|t-1} &= \mathbb{E}[(z_t - z_{t|t-1})^2|k_1^{t-1}, \sigma^2_\epsilon, z_0]\\
z_{t|t} &= \mathbb{E}[z_t|k_1^{t}, \sigma^2_\epsilon, z_0]\\
\sigma^2_{t|t} &= \mathbb{E}[(z_t - z_{t|t})^2|k_1^{t}, \sigma^2_\epsilon, z_0]\\
\ell_t &= \frac{k_t - np_{t|t-1}}{p_{t|t-1}(1-p_{t|t-1})}\\
\frac{\mathrm{d}p_t}{\mathrm{d}z_t} &= \frac{x_t(1-p_t)\exp(x_t)}{\exp(x_t)+1}\\
g_t &= \frac{x_{t|t-1}\exp(x_{t|t-1})}{\exp(x_{t|t-1})+1}(1-p_{t|t})
\end{aligned}$$

We computed MVPs separately for whiskers and paws. To initialize the algorithm, an EM-algorithm was used on the four minutes of baseline data to find parameters σ^2_ϵ and z_0.

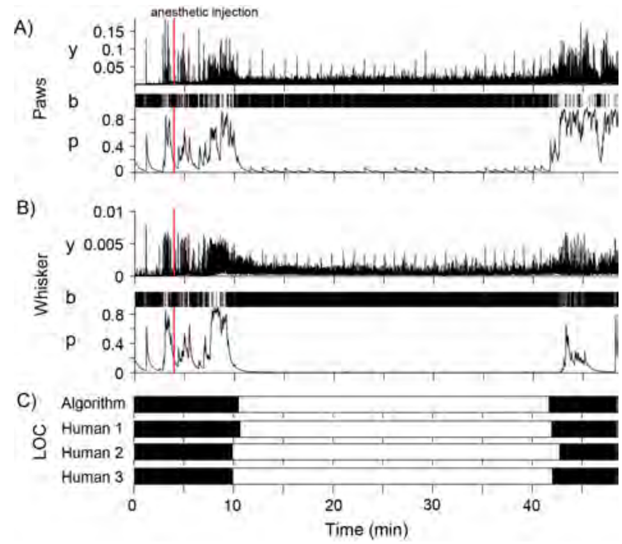

Fig. 4. Example of data processing. Panel A (B) show the median optical flow y obtained from the movement of paws (whiskers) in a video using the Lucas-Kanade derivative of Gaussian algorithm, the movements detected from these b, and the associated MVPs (p). Panel C shows the periods of LOC identified by our algorithm and three human observers.

D. Identification of LOC and performance assessment

We defined LOC as having a MVP of less than 0.1 in either whiskers or paws and identified the period of LOC in each animal using the fully automated algorithm described in Sections II-B and II-C. We also defined the minimal time for a period of LOC identified to be at least 3 minutes. We compared the performance of the algorithm to the annotations of LOC and non-LOC periods provided by three independent and experienced human observers who were provided with the videos only. We defined human consensus as having agreement between at least two of the three observers. Then we computed the percentage time when there was inter-human A_{hh}, human-algorithm A_{ha}, and algorithm-human consensus agreement A_{ac} on the labels of LOC or non-LOC. From this analysis, we obtain 7 comparisons. Each of these is characterized by a distribution of the percentage time in which the pair compared was in agreement. Finally, we computed the 95% confidence interval for the median value of each of these distributions using non-parametric bootstrap. We defined two distributions as statistically significant only when there is no overlap between the confidence interval of their median values.

III. Results

We conducted 10 experiments in total. Dexmedetomidine was used in one half of the experiments and ketamine in the other half. The duration of the experiments ranged from 19.7 – 48.5 min with a median of 30.2 min. We processed the videos using the algorithms described in Sections II-B and II-C, and automatically identified periods of LOC using the criteria described in Section II-D. Figure 4 shows the whisker and paw median optical flow, movement detected, and MVP, as well as the LOC identified by the algorithm and human observers for one experiment.

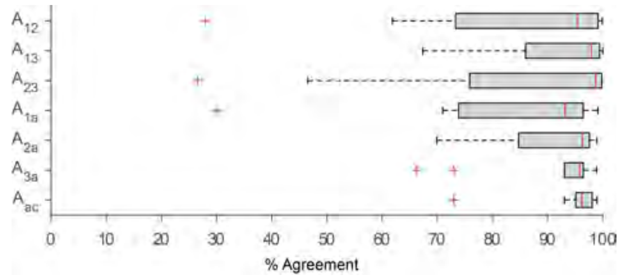

Fig. 5. Boxplot showing distributions of inter-human agreement ($A_{12}, A_{13}, \text{and} A_{23}$), human-algorithm agreement ($A_{a1}, A_{a2}, \text{and} A_{a3}$), as well as algorithm-human consensus agreement A_{ac} based on data obtained from 10 experiments.

We show a box plot summarizing inter-human agreement A_{hh}, human-algorithm agreement A_{ha}, and algorithm-human consensus agreement A_{ac} for all experiments in Fig 5. The whisker length is set to 1.5 times of the interquartile range (IQR). Table I summarizes the median, 95% confidence interval (CI) of the median, mean, and standard deviation (std) for each of the seven comparisons. None of the comparisons made were statistically different from the others. However, we can see that A_{ac} has the smallest 95% CI of the median and standard deviation while A_{23} has the largest 95% CI of the median and standard deviation. Interestingly, the agreement between the algorithm and human consensus was less variable than the agreement between the individual human observers and human consensus. Therefore, the results indicate that our algorithm perform at least as well as human observers, and has improved precision when compared with individual human observers.

IV. Discussion and Conclusion

We propose a new behavioral assay based on LOM for examining LOC in head-fixed rodents where the traditional assays such as LORR cannot be used. As evident from the variability of the inter-human agreement in our results, the task of identifying LOM in whiskers and paws is challenging. This is probably because such movements are much less obvious and harder to assess than LORR. The process of having humans manually determine LOC by watching the video is also labor intensive and subjected to bias [12]. Therefore we are motivated to develop an automated algorithm to perform this task.

We designed and implemented an algorithm based on optical flow measures of motion and point-process filtering toh estimate a novel index called movement probability. We used the movement probability to detect LOC in 10 experiments, and confirmed that the proposed behavior assay based on LOM is tractable. By comparing with human annotated period of LOC versus non-LOC, we showed that the algorithm is as accurate and more precise. The algorithm was also applied successfully to recordings made at low frame-rates and moderate resolution. Therefore, it is useful without using cameras with high resolution and frame-rates.

Comparison	Median	95% CI of median	Mean	Std
A_{12}	95.4	[73.3 99.2]	82.9	23.4
A_{13}	97.9	[73.3 99.4]	91.7	12.1
A_{23}	98.7	[75.9 99.8]	84.3	26.6
A_{1a}	93.1	[73.8 96.5]	83.2	21.3
A_{1a}	96.3	[74.3 98.4]	90.6	10.6
A_{1a}	95.8	[73.0 96.5]	90.9	11.4
A_{ac}	96.2	[95.1 98.9]	94.3	7.7

TABLE I

In this analysis, we have limited ourselves to identifying periods of LOC vs non-LOC for an initial proof-of-concept. However, the movement probability is not a binary measure but a continuous metrics and can be used to characterized more subtle behavioral changes. This can be exploited in future work to refine our current analysis of LOC, distinguish between different depths of sedation during anesthesia, and characterize other relevant behavioral states such as paradoxical excitation.

Finally, our proposed method will enable the combination of behavioral and invasive neurophysiological measures in head-fixed rodents. This is crucial for gaining new insights about the neural mechanism of anesthesia and consciousness.

References

[1] K. F. K. Wong, A. C. Smith, E. T. Pierce, P. G. Harrell, J. L. Walsh, A. F. Salazar, C. L. Tavares, A. Cimenser, M. J. Prerau, E. A. Mukamel, A. Sampson, P. L. Purdon, and E. N. Brown, "Bayesian analysis of trinomial data in behavioral experiments and its application to human studies of general anesthesia," vol. 2011, pp. 4705–4708.

[2] C. Koch, M. Massimini, M. Boly, and G. Tononi, "Neural correlates of consciousness: progress and problems," vol. 17, no. 5, pp. 307–321.

[3] N. Kleitman, "Sleep, wakefulness, and consciousness," vol. 54, no. 4, pp. 354–359; discussion 360.

[4] F. J. Flores, K. E. Hartnack, A. B. Fath, S.-E. Kim, M. A. Wilson, E. N. Brown, and P. L. Purdon, "Thalamocortical synchronization during induction and emergence from propofol-induced unconsciousness," *Proceedings of the National Academy of Sciences*, vol. 114, pp. E6660–E6668, Aug. 2017.

[5] S. B. Kodandaramaiah, F. J. Flores, G. L. Holst, A. C. Singer, X. Han, E. N. Brown, E. S. Boyden, and C. R. Forest, "Multi-neuron intracellular recording in vivo via interacting autopatching robots," *eLife*, vol. 7, p. e24656, Jan. 2018.

[6] P. W. Wright, L. M. Brier, A. Q. Bauer, G. A. Baxter, A. W. Kraft, M. D. Reisman, A. R. Bice, A. Z. Snyder, J.-M. Lee, and J. P. Culver, "Functional connectivity structure of cortical calcium dynamics in anesthetized and awake mice," *PloS One*, vol. 12, no. 10, p. e0185759, 2017.

[7] B. D. Lucas and T. Kanade, "An iterative image registration technique with an application to stereo vision," pp. 674–679, 1981.

[8] J. L. Barron, D. J. Fleet, and S. S. Beauchemin, "Performance of optical flow techniques," *International journal of computer vision*, vol. 12, no. 1, pp. 43–77, 1994.

[9] M. Brandon Westover, M. M. Shafi, S. Ching, J. J. Chemali, P. L. Purdon, S. S. Cash, and E. N. Brown, "Real-time segmentation of burst suppression patterns in critical care EEG monitoring," *J. Neurosci. Methods*, vol. 219, pp. 131–141, Sept. 2013.

[10] A. C. Smith and E. N. Brown, "Estimating a State-Space Model from Point Process Observations," *Neural Computation*, vol. 15, pp. 965–991, May 2003.

[11] J. Chemali, S. Ching, P. L. Purdon, K. Solt, and E. N. Brown, "Burst suppression probability algorithms: state-space methods for tracking EEG burst suppression," *J Neural Eng*, vol. 10, p. 056017, Oct. 2013.

[12] A. Tversky and D. Kahneman, "Judgment under uncertainty: Heuristics and biases," *Science*, vol. 185, no. 4157, pp. 1124–1131, 1974.